IEEE Access
Multidisciplinary | Rapid Review | Open Access Journal

Received October 21, 2020, accepted November 11, 2020, date of publication December 7, 2020,
date of current version December 23, 2020.

Digital Object Identifier 10.1109/ACCESS.2020.3043206

Detecting Motion in a Room Using a Dynamic Metasurface Antenna

ALEXANDER X. OESTERLING, MOHAMMADREZA F. IMANI, (Member, IEEE), OREN S. MIZRAHI, (Graduate Student Member, IEEE), JONAH N. GOLLUB, (Member, IEEE), AND DAVID R. SMITH, (Senior Member, IEEE)

Center for Metamaterials and Integrated Plasmonics, Department of Electrical and Computer Engineering, Duke University, Durham, NC 27708, USA

Corresponding author: Alexander X. Oesterling (axo@duke.edu)

This work was supported in part by the Advanced Research Projects Agency-Energy (ARPA-E), US Department of Energy, under Grant DE-AR0000937.

ABSTRACT Sensing motion and distinguishing its source as human or nonhuman, with high precision, has tremendous applications in a variety of areas from health monitoring to energy efficiency. One strategy to achieve this goal is to detect the small motion of breathing, which is a consistent indicator of human presence. Among the many smart sensing schemes proposed, microwave and RF sensors have shown great promise due to their simplicity, privacy, and effective range. In this paper, we propose the use of a dynamic metasurface antenna (DMAs) as an alternative hardware platform for sensing motion inside a residential setting using microwave signals. The proposed device is a single-port planar cavity that excites an array of electronically-tunable metamaterial elements. The DMA can generate spatially diverse patterns at a single frequency, avoiding complexities related to wideband operation or high hardware costs of antenna arrays. We demonstrate that it is capable of detecting minute movements, such as breathing emulated by a mannequin, to distinguish human presence. This motion can be detected whether the target is in the the sensor's direct line of sight or out of the direct line of sight. Furthermore, we show that the DMA sensing platform requires a single noise-floor calibration and can operate in different room geometries or configurations (e.g. when furniture is displaced). The proposed DMA-sensor with its single frequency operation and simple hardware is an appealing alternative hardware for intruder detection, human presence detection/activity recognition in smart homes, or seamless health monitoring.

INDEX TERMS Microwave sensors, electromagnetic metamaterials, radar detection, energy efficiency, radio frequency (RF).

I. INTRODUCTION

Detecting the presence, condition, and actions of humans inside residential settings is becoming a topic of great interest in smart-home technology, environment-monitoring, assisted living, precision health, and energy efficiency [1]–[4]. In 2015, the residential sector consumed 9.114 quadrillion BTUs of power, much of it wasted by leaving unnecessary functions such as air conditioning and lighting on while people are absent from their homes [5]. A human presence sensor could potentially reduce power consumption by 30% [3]. Furthermore, such a sensor could be used to aid in monitoring the health of a room's occupants, such as detecting when an elderly person falls and needs medical attention [6] or when abrupt changes to the breathing rate occur [7].

The associate editor coordinating the review of this manuscript and approving it for publication was Kuang Zhang.

There are three major technical approaches when it comes to human detection: infrared (IR) [8]–[10], optical [7], and RF-based sensors [2], [11], [12]. The most widespread solution available on the market employs IR pyroelectric sensors, which offer a low cost hardware, but incur high false negatives—to the point that they become a nuisance to the users. More recent solutions involve optical cameras. While these cameras can offer more information than just human presence, capturing pictures inside houses comes with privacy concerns. Further, both optical and IR sensors cannot operate around corners or through furniture and other obstructions. RF signals, however, can surmount these challenges: electromagnetic waves at these frequencies can penetrate optically-opaque materials (such as furniture, blankets, etc.), have low health risks, and do not encounter the potential privacy violations of optical light based detectors. These benefits have triggered a growing

interest in RF and microwave technology for human presence detection [1].

Microwaves and RF signals are reflected by the human body. As a result, RF sensors need a mechanism to differentiate the human body from common reflective objects in a residential setting. To do that, RF sensors usually detect human-associated movement (which is distinct from all objects in a room). Within the RF-based sensors for human presence detection, there are two overall categories of sensing schemes: 1) Radar based sensors [2], [13], [14] and 2) Wireless Network based sensors [12], [15]–[17]. Radar-based systems detect the Doppler shift induced on a wideband signal; WiFi based systems track changes to the channel state information over different subcarriers as a result of human movements. Both systems have shown great promise in detecting human presence and even identifying their movement [18]. However, these techniques still have certain practical challenges to overcome. The wide operating bandwidth of radar systems must obey FCC governmental policy on consumer radio products, which can limit their range. In addition, wideband systems are usually more expensive and complicated, and as a result, widespread use of radar-based sensors may not be economically feasible. The general advantage of WiFi-based systems is that they can leverage existing infrastructure and the associated economies of scale. However, this advantage also exposes the human-presence detection data to the security vulnerabilities of WiFi systems. For example, the personal location information of inhabitants and their habits can be compromised because the antenna and its processing are connected to the internet [1]. An alternative approach is to use dedicated wireless network devices solely for human presence detection, but this alternative can interfere with other WiFi devices in a building. In either case, the diversity of information over WiFi subchannels is limited, which hinders their ability to detect small human movements such as breathing. To overcome this problem, it has been suggested to augment WiFi-based systems with multiple antennas or deploy them at different locations, but that comes with an increase in their associated cost and complexity [19].

A related but distinct method to detect motion based on RF sensors was recently proposed in [16], [20]. In this method, the residential setting is viewed as a cavity with many modes; the changes in the modal distribution are then monitored to detect motion [21], [22]. Unique to this proposed idea was the use of a dynamic metasurface antenna (DMA) operating at a single frequency. In general, DMAs consist of an electrically large waveguide or cavity fashioned with individually-addressable metamaterial elements [23]–[25]. When microwaves are injected into this structure, they couple to the metamaterial elements and radiate into a region of interest. The overall radiation pattern, which is a superposition of fields generated by the many metamaterial elements, can thus be altered by changing the tuning state of the metamaterial elements. These reconfigurable, spatially diverse patterns have shown great promise in computational microwave imaging schemes, in which each measurement provides enough independent information regarding a scene such that an image can be reconstructed [23]–[27]. In [20], the DMA's spatially diverse patterns were shown to offer an alternative for the tradeoff between spatially diverse (WiFi sensors) and frequency diverse sensors (radar-based sensors). In fact, the single-port DMA can realize a sufficiently diverse number of measurements of a room's modal distribution at a single frequency [20], [28]. This feature was recently experimentally verified using scans of the field generated by a DMA in a mock room [29]. However, [29] did not demonstrate an increase in the ability to detect motion as a result of this information diverse pattern. In [20], a DMA was shown to detect motion in a few non-line-of-sight (NLOS) locations in a lab setting (a metallic cavity), but a complete coverage map was not reported. This paper extends the results of these two papers and examines the DMA's ability to detect motion within a mock room, emulating a real-life setting.

We use the same mock room as in [29] and the same DMA which is described in [30]. To examine motion detection in a controlled manner, we use a moving mannequin torso inside the room. The torso is affixed to a motion stage, and programmed to move periodically over 2 cm, emulating human breathing. We examine the fluctuation in the signal as a result of this motion for two cases: one in which a DMA with different radiation patterns is used to probe the room, and one in which a DMA with a fixed radiation pattern is used. The latter emulates the case of fixed pattern antennas such as those used in a WiFi system or radars. By placing the mannequin in different locations in the room, we show that using the reconfigurable radiation patterns generated by the DMA to probe the room significantly increases the motion detection fidelity throughout the room. We also demonstrate that the improved fidelity is achieved even when the mannequin's orientation changes. Finally, we show that the motion sensing scheme based on the DMA requires only a one time calibration (which entails measurement of the noise floor) and is independent of the room geometry and content.

This paper is organized as follows. In Section II of this paper, we detail our experimental setup and our data collection procedure. We then go on in Section III to discuss the mathematical analysis and post processing of our collected data. Finally, in Section IV we discuss these results and move on to consider future steps for our research in Section V.

II. EXPERIMENTAL SETUP: HARDWARE

A. INDOOR TESTING CONFIGURATION

We use a life-size mock room to examine the DMA's capability to detect motion. This room, whose layout is shown in Fig 1, is built of plywood walls and ceilings, similar to a room in a typical residential building. The plywood walls are half-inch-thick and are supported by $2' \times 4'$ beams. The exterior of the room is padded with microwave absorber to isolate the experiment from surrounding equipment and radiation that may interfere with the data collection. The room has an L shape, with a plywood door and most of the ceiling covered

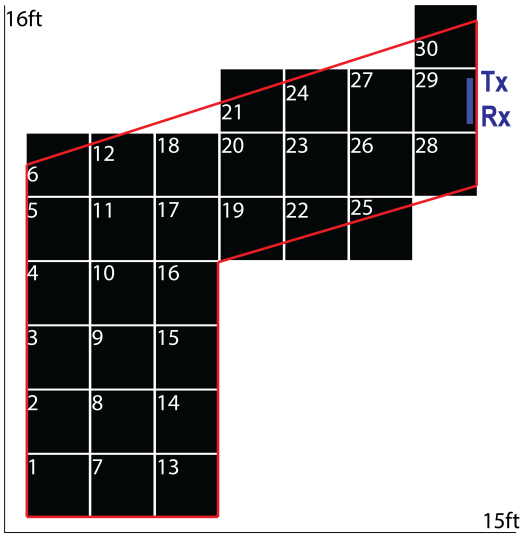

FIGURE 1. A top-down view of the mock room with a grid of locations. The red lines represent the actual dimensions of the room.

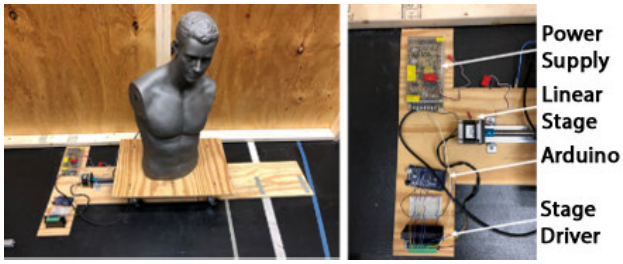

FIGURE 2. Mannequin covered in conductive paint and mounted on a moving stage.

in plywood. The room is divided into a grid of 30 locations. On one end of the L-shaped room is the DMA transmitter and a printed dipole receiver. Based on the location of transmitters and receivers, we can consider the other side of the L-shape to be non-line-of-sight (NLOS) since this region does not have a direct view of the DMA and the receiving dipole. The rest of the room is in the line-of-sight (LOS) of the DMA. The DMA is excited by one port of a VNA (outside of the room). The signal bounces around the room and is collected by the printed dipole receiver connected to the other port of the VNA. To realize a controlled movement pattern similar to what one would expect in a real-life scenario while keeping the motion consistent across all studies, we place a mannequin torso on an Arduino-controlled moving stage (see Fig. 2). The mannequin is covered in conductive paint that mimics the reflection of the human body, which acts as a good reflector (similar to metals) at microwave frequencies. Emulating a human body with a conductive paint covered mannequin is common practice at microwave frequencies, as exemplified in experiments on microwave security screening (see for example [31] and references therein). This mannequin is programmed to emulate a human breathing motion, as detailed in Subsection II.C.

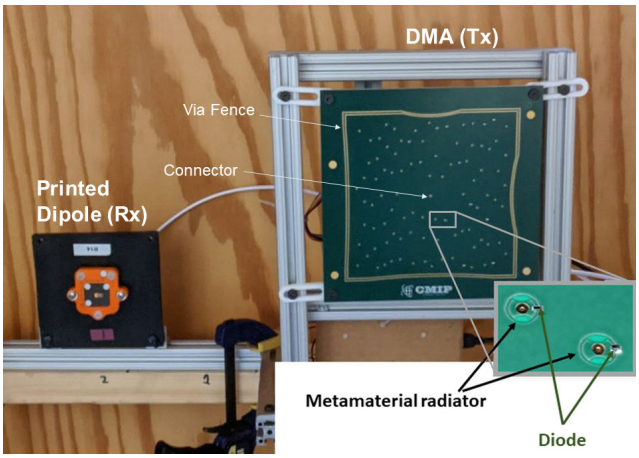

FIGURE 3. DMA mounted in the corner, serving as transmitter.

B. DYNAMIC METASURFACE ANTENNA

The DMA used in this experiment is described in detail in [26], [30] and is shown in Fig. 3. This device is fabricated from a dual-sided copper-clad printed circuit board (PCB, 60 mil thick Rodgers 4003). An electrically-large cavity—approximately 15 $cm \times 15$ cm—is defined by the two planar, copper layers and an irregularly shaped via cage. A coaxial connector inserted into one of the plates feeds microwaves into the cavity. On the opposite copper side, there are 96 randomly-placed metamaterial radiators [32]. Each radiator has a diode that is individually addressable [24], allowing each metamaterial radiator to be set in an on (radiating) or off (non-radiating) state. By changing the selection of radiating and non-radiating (on and off) elements, spatially diverse radiation patterns can be generated and selected by external control [26], [30]. We refer to each configuration of *on* and *off* metamaterial elements as a *mask* consisting of 96 bits. This device has already been proven experimentally to generate diverse patterns at 19 GHz in close range for imaging [30] as well as inside a room [29]. In this paper, we use a similar set of masks as in those studies; specifically, we consider masks with about half of the radiators turned on. The radiating elements for each mask are distributed randomly across the DMA aperture. The DMA used in our studies is designed to operate between 17.5-22 GHz. In this work, we use the single frequency of 19 GHz because the results of [30] demonstrated that the device exhibits higher pattern diversity at frequencies around 19 GHz. However, the proposed DMA can be redesigned to operate at different frequencies if so required. For example, at around 5.8 GHz, we can use mature WiFi technology and leverage lower propagation losses. This comes at the cost of higher interference, lower sensitivity, and a larger DMA. At higher frequencies (e.g. 28 GHz), we will have higher sensitivity, but will suffer from high propagation losses. The proposed operation (using pattern diversity at a single frequency) would work at any frequency range, and the choice is more related to regulatory and cost/sensitivity, and is beyond the scope

of this work. Here, we want to demonstrate the utility of pattern diversity and use a DMA to realize that to detect motion.

C. PROGRAMMED MOTION

The DMA can be programmed to change its masks at a rates up to a KHz with dedicated hardware. As a result, it can capture changes inside a room at a rate much faster than usual movements caused by humans (which are usually at a few Hz). In this manner, the DMA can be expected capture the motion signatures of different movements and deduce human presence. However, in the current setup, the DMA is controlled by a PC, which also controls a VNA as well as the mannequin. As a result of the communication overhead, we cannot measure the data in real time. Instead we take measurements in a stop-motion fashion. This manner of data acquisition has another important advantage: we can conduct different measurement/sensing schemes in a controlled manner with the same motion pattern. This setup thus allows us to achieve fair comparisons between fixed-pattern measurements (similar to the case of WiFi systems) and reconfigurable-pattern measurements using different masks (i.e. our proposed technique).

In our studies, we use the following measurement sequence:

1) The Arduino controlling the mannequin initiates movement over a defined step
2) The DMA configures its metamaterial radiators to a certain mask
3) The VNA sends a microwave signal through the DMA and receives it through the printed dipole, recording the coupling between the two
4) Steps 2 and 3 repeat for each mask configuration specified in the script, and then the process restarts at step 1 for each new time step

The mannequin is programmed to move a pre-calculated distance to simulate the speed of an actual human breathing. We take time steps of 0.1 seconds, and assume a sinusoidal breathing motion with frequency of 0.2 Hz and amplitude of 2 cm.

We use the DMA in two different schemes: 1) for each time instance, the DMA iterates through M unique masks, and 2) we select one fixed mask and measure the received signal M times. The latter case is similar to what happens when a fixed-pattern antenna (similar to WiFi routers or radar systems) is used for sensing. Note that by using the same number of measurements, we ensure both measurement schemes have equal noise averaging benefits.

The output of the measurement sequence described above is an $N \times M$ matrix, with M corresponding to the number of masks and N corresponding to the total length of time in tenths of a second, or number of samples in the time dimension. In the next section, we describe the process to analyze this data sequence.

III. EXPERIMENTAL SETUP: SOFTWARE

A. ANALYSIS

To deduce the motion of the mannequin from the data collected by the receiver, we propose investigating the fluctuations in the measured signal. Physically speaking, the wave collected by the receiver consists of stationary and dynamic parts [33], [34]. The former corresponds to the waves that bounce around and do not interact with the moving scatterer (mannequin in this case). This portion also includes the direct coupling between the transmitter and the receiver. The latter is the *dynamic component*, composed of waves that have interacted with the mannequin. To deduce the presence of mannequin motion, we need to extract the dynamic component. A simple method is to subtract the average of the signal over time from the received signal, or

$$C(t, m) = R(t, m) - R_{avg}(m) \tag{1}$$

where R represents the raw data from our sensor in matrix form and C represents the dynamic component.

To investigate the fluctuations of the dynamic component, C, we then focus on fluctuation of the received signal in subsequent time instances. This is equivalent to taking the discrete time derivative and multiplying by Δt. Because of our stop motion setup, Δt is constant across all data:

$$F(t, m) = \dot{C}(t, m)\Delta t = C(t + 1, m) - C(t, m) \tag{2}$$

The resulting matrix, F, denoting temporal fluctuation, is an $N - 1 \times M$ sized matrix.

In ideal settings and without noise, any nonzero values in the fluctuation matrix *should* correspond to motion within the room. However, these fluctuation values can be small and dominated by the noise at the receiver. This is especially the case here since we are trying to detect small motion caused by a mannequin torso emulating breathing. To overcome this challenge, we need to obtain multiple independent measurements of the motion. Two overarching techniques have historically been suggested for this purpose: 1) Obtain measurements of the room by placing transmitter(s) and/or receiver(s) at different locations. This method results in *spatial diversity* that can be realized by using multiple antennas or sensors. 2) Use information obtained over different subcarriers of a communication channel (i.e. *frequency diversity*). We can consider ultrawideband radar as an extreme example of this case.

Here, we propose an alternative methodology: leverage the tunability (i.e., the dynamically reconfigurable directivity) of the DMA to generate many spatially diverse patterns to emulate *spatial diversity*. An intuitive explanation of this idea is as follows: each radiation pattern probes the room differently, and as a result, may or may not interact with the dynamic scatterer. By increasing the number of patterns, we increase the possibility that the received signal to contains signatures of the fluctuation caused by the motion.

Mathematically, we want to extract a vector of size $N - 1$, containing 1's for "detection" or 0's for "no detection",

of motion from the $N - 1 \times M$ sized fluctuation matrix. A variety of techniques are available to transform this M-dimensional matrix to a 1 dimensional one (ignoring temporal dimension). Here, we aggregate each mask's fluctuation by taking the standard deviation of the masks' fluctuation:

$$F_{agg}(t) = std(F) \tag{3}$$

We then compare this aggregate to the aggregate of a period of time during which there is no motion in the room. In practice, this could be considered as a *calibration* measurement taken at the installation of an occupancy sensor. We then threshold the measurement, defining motion to be when the standard deviation of the measurement is greater than the standard deviation of the motionless period.

The analysis above only yields a boolean value for each time instance indicating motion or no motion. In many instances, we are interested in recovering more information about the source of motion such as its source and quality. For example, by retrieving the temporal characteristics of motion, and comparing them with known signatures, we can deduce the source of the motion to be a human or non-human. In our study, if we can obtain an estimate of the motion to be with a time dependence corresponding to a typical breathing rate, then we can distinguish it from potential non-human motion.

To deduce the temporal characteristics of the motion, we examine the temporal characteristics of the fluctuation vector, $F_{agg}(t)$. Since this variable is corrupted by high frequency oscillations due to noise (especially when the return signal is small), we apply a low pass filter by taking the moving-average of the fluctuation signal using Matlab's `smooth` function with a window of 5 (corresponding to 0.5 seconds) to attenuate noise greater than 1 Hz. Note that a similar process can be applied in real life settings since we know the breathing rate is usually below 1 Hz. In the last step of our analysis, we take the Short-time Fourier transform using Matlab's `pspectrum` function. Note the presence of temporal banding in the right column of figures in 4. This occurs because the function computes Short-time Fourier transforms in windowed segments, which correspond to the discrete bands we see in the generated figure.

IV. EXPERIMENTAL RESULTS

We begin by examining the received signals in two illustrative locations: one in a LOS and one in a NLOS location. To start, we keep our mannequin facing in directly towards the DMA. Later, we will define this orientation as 90 degrees and investigate other angles of orientation. Building on the results of this study, we then examine the entire room. Lastly, we examine the impact of the orientation of the mannequin motion and adding clutter to the mock-room environment.

A. LINE-OF-SIGHT DETECTION

To examine motion detection in LOS, we place the mannequin in location 16 of the layout shown in Fig. 1. The standard deviation of the fluctuation signal, F_{agg}, computed using 300 unique masks, is shown in Fig. 4 A.I.. We see a clear periodic signal as the mannequin moves back and forth. We also observe high fidelity in detecting motion since the variation of the signal is clearly above the noise floor. This is expected since we have placed the mannequin in the direct LOS of the DMA and the receiver. Next, we examine the fidelity of characterizing motion. The steps taken in this process, as outlined in the previous section, are visualized in Fig. 4, Row I. First, we apply a low pass filter to eliminate any high frequency noise (see Fig. 4 B.I). We then investigate the signal in the frequency domain. The overall power spectrum and its temporal evolution are shown respectively in Figs. 4 C.I and D.I. As mentioned previously, the temporal banding visible in 4 D.I. a result of the windowed Short-Time Fourier transform (STFT) method used for analysis. We see an evident peak in the power spectrum at 0.4 Hz. This value is twice the periodicity at which the mannequin is programmed to move. This doubling of periodicity is due to the fact that our processing procedure outlined in the previous section is based on the standard deviation, which is always a positive number. Intuitively, the standard deviation of fluctuation peaks when the mannequin is at the edges of its movement. Therefore, our results show twice the mannequin's moving frequency, or 0.4 Hz for our 0.2 Hz motion.

B. NON LINE-OF-SIGHT DETECTION

Next, we examine motion detection quality in NLOS by placing the mannequin in location 14 of the layout shown in Fig. 1. We used the same 300 masks as in the LOS case. The results are shown in the second row, or Fig. 4 Row II. While we detect motion in few instances, the overall fidelity is much lower than the previous case. This is expected since the power of the received signal in NLOS is much lower. To improve upon these results, we increase the number of masks to 800. The results are shown in Fig. 4 Row III. We see an evident improvement in detecting motion as the majority of the received fluctuation signal is above the noise floor (Fig, 4 A.III). The periodic nature of the standard deviation of the fluctuation signal, F_{agg}, is also visible. After applying low-pass filtering (Fig. 4 B.III), the periodic nature of motion becomes more evident. To further characterize this motion, we again inspect the filtered signal in the frequency domain. Figs.4 C.III and D.III illustrate the power spectrum and temporal evolution respectively. Despite being NLOS, there is still a clear peak at 0.4 Hz in the power spectrum. Furthermore, we can observe this prominent peak over the whole duration of the motion.

To illustrate the fact that it is DMA's spatially distinct patterns that help with improving detection fidelity (and it is not a mere averaging to reduce the impact of noise), we have also examined the same motion using 800 identical patterns. It is worth noting that using a controlled stop-motion sequence of motion allows us to conduct a fair comparison of these two cases. This case is essentially similar to conventional systems where a simple non-reconfigurable antenna is used. The results of this case are shown in 4 Row IV. We clearly see that using 800 identical masks does not help with detection

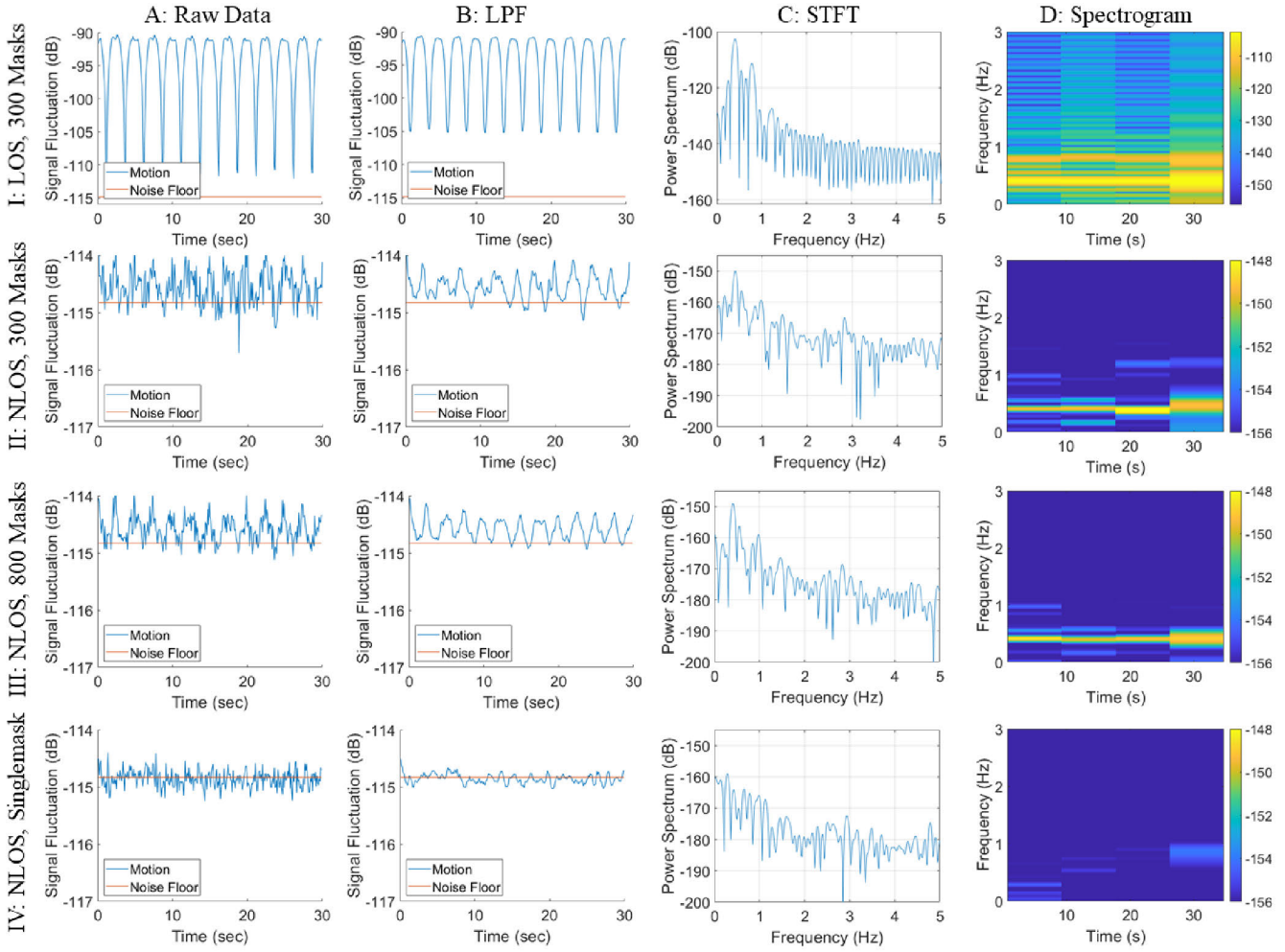

FIGURE 4. **Results comparing LOS and NLOS locations as well as the impact of mask diversity on detection fidelity. LOS detection is easier than NLOS detection, but by increasing the mask diversity, we can still confidently detect motion around the corner from our DMA. The LOS location was 16 and the NLOS location was 14 as seen on the map of the room in Fig. 1.**

fidelity, and it is the spatially distinct patterns of the DMA that increase the fidelity of detection.

C. COVERAGE MAP

Having established the DMA's utility in detecting motion in a LOS and a NLOS location, we collect data for the whole room to populate a coverage map. To do that, we place the mannequin in each of the 30 locations shown in Fig. 1, and conduct the same motion test. Note that we employ the same stop-motion sequence for the mannequin at all locations, and thus obtain a fair comparison over the whole room. We apply the same processing described in Section III.A to the data collected for each location. For our coverage maps, we use 300 masks for LOS and 800 masks for NLOS locations, rather than an ideal 800 for all locations. There are three reasons for this; first, an 800 mask measurement in stop-motion takes 10 hours in real life, whereas a 300 mask measurement only takes 4, so in the interest of time, we decided that 300 masks to be sufficient for LOS detection. Secondly, the results above show that 300 masks is sufficient to detect motion in NLOS cases, but 800 masks helps to improve clarity. Finally, as we transition to real-time studies, the tuning frequency of the DMA becomes a factor requiring tradeoffs between increased masks and fidelity, and tuning speed. We first examine the ability to detect motion by defining a variable proportional to the number of instances the measured fluctuation was above the noise floor; this value allows us to quantify the fidelity of detecting motion. The results of this study are plotted in Figs 5a, b, and c for three different cases: a) the best result possible using the DMA where we used 800 unique masks for NLOS and 300 unique masks for LOS. Again, note that 300 masks is sufficient for the LOS location and using more than would only have resulted in more time consuming measurements. Fig 5 (b) shows the case where we used only 100 unique masks for all the locations. (c) shows the case where we used the same mask, 800 times in NLOS and 300 times in LOS. At every time instance t, we check if the fluctuation of the signal is greater than the noise floor, and

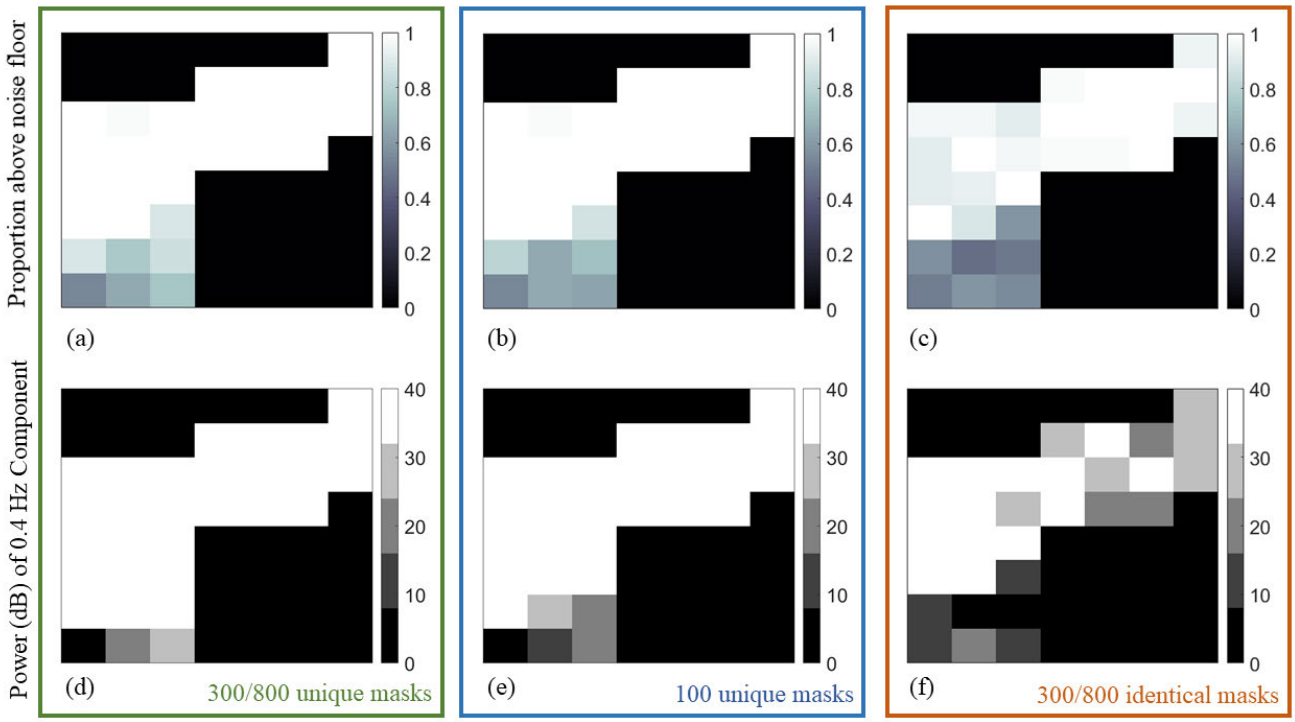

FIGURE 5. Coverage maps for mock room at specific mask values. Maps (a) and (d) correspond to 300 mask measurements for LOS locations and 800 mask measurements for NLOS locations. Maps (b) and (e) correspond to 100 mask measurements in both locations. Maps (c) and (f) correspond to single mask measurements in both locations. The top row shows the proportion of data points above the noise floor, while the bottom row shows the relative power of the 0.4 Hz signal.

then sum up all time points to create a ratio of data points which are above the noise floor. This is a representation of our confidence of detecting motion in the room.

The results in Figs 5a, b, and c show several interesting features. The first observation is that the DMA, except for the very extreme corner (bottom left of Fig. 5a), yields detection fidelity above 50%. This is in contrast to the case where we use the identical mask 800 times; as shown in Fig. 5 (c), traditional detection schemes are only suitable for LOS of locations. Comparing 5 (a) and (b), we can see the improvement achieved by increasing number of masks.

Next, we investigate fidelity in detecting temporal motion characteristics. Toward this goal, we define a variable to quantify our ability to detect this known periodicity: we take the difference between the power of the signal in the frequency domain at 0.4 Hz and the average power of the signal in the frequency domain in each location (Fig 5d, e, and f). We use the same STFT as before to extract frequency information. As seen in (d), the best results occur when the DMA uses more masks, and we are able to see distinct spikes in power at the target frequency. Fig. (e), where we measure with 100 masks continues to demonstrate the efficacy of the DMA in LOS locations and a few NLOS locations, but fails to measure as clearly as (d) because of its lack of masks. Finally, (f), where we measure with 800 repeated masks to emulate traditional sensing schemes, demonstrates a lack of clear spikes at the target frequency even in LOS locations, illustrating the necessity of the DMA sensing system to extract relevant motion from a room.

D. IMPACT OF NUMBER OF MASKS

Up to now, We have seen increasing number of masks from 300 to 800 significantly improve detection fidelity, especially in NLOS locations. However, we have not investigated the correlation between number of masks and detection fidelity. The answer to this question can determine the ideal number of masks required for a measurement. From a practical standpoint, this is important because keeping the number of masks low is valuable for acquisition rate and computation and storage concerns.

To examine the impact of increasing the number of masks, we plot the proportion of measurements above the noise floor while varying the number of masks being processed. This is the same metric we used for the coverage maps in Fig. 5. We plot the ratio of measurements above the noise floor over the duration of motion for two LOS (16, 23) locations and two NLOS (2, 14) locations as we increase the number of masks. As shown in Fig. 6, we see a general trend of increasing fidelity as we increase the number of masks. However, the trend in increase is not identical: for the LOS cases, the proportion almost immediately reaches 1, showing that again, the fluctuation (and consequently presence of motion)

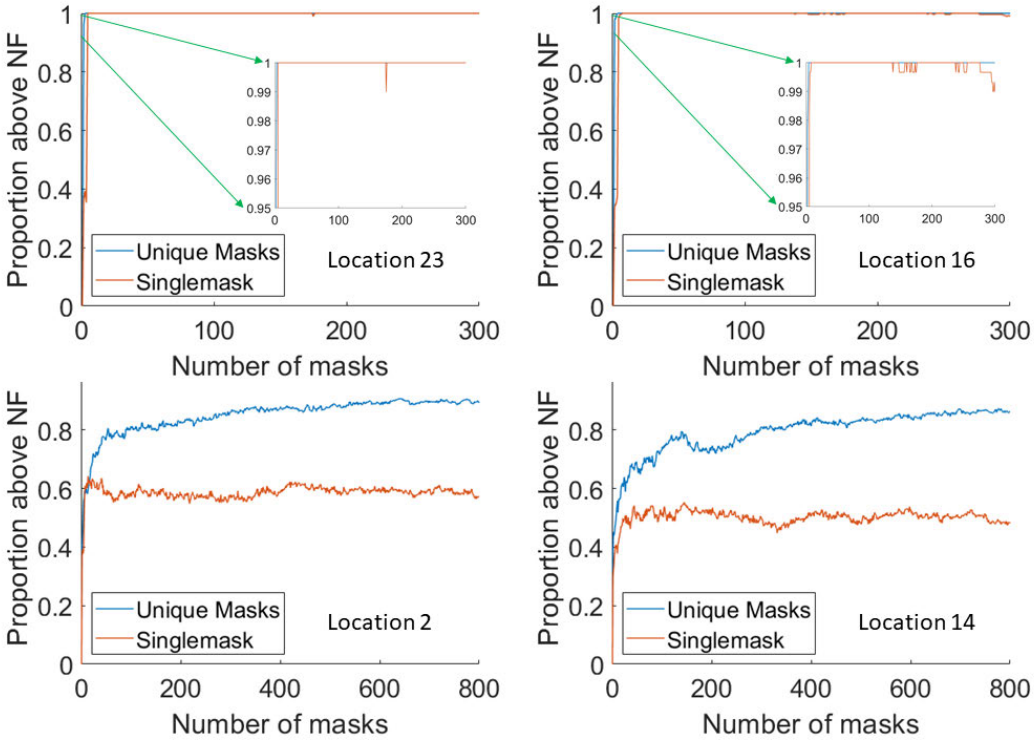

FIGURE 6. Proportion of fluctuation signal above noise floor vs masks. Each plot is labeled with the location it came from. The top row (Loc. 16 and 23) are from LOS locations whereas the bottom row (Loc. 14 and 2) are from NLOS locations. Magnified plots for top row are scaled to proportions from 0.95 to 1.

is easily extracted from the signal in LOS cases. On the other hand, we see a more gradual increase in fidelity as we increase number of masks in NLOS locations. We identify a knee in each plot, but each happens at different number of masks. We also see a saturation effect: increasing masks more than 800 does not improve detection beyond around 80% in those plots.

Another interesting observation is the single-mask case. While in LOS its performance is satisfactory, in the NLOS, it never reaches desired performance. These plots clearly illustrate two things. First, detection fidelity increases with the number of unique masks used (and it is not a result from simply noise averaging), and secondly, increasing number of masks starts to have diminishing returns. We should select the number of masks based on the acquisition rate, desired level of detection, and computational and storage requirements.

E. MANNEQUIN ORIENTATION

In the studies presented above, the orientation of the mannequin was, more or less, kept the same. In this subsection, we examine the impact of orientation on the motion detection fidelity and the utility of the DMA for different mannequin orientations. For these experiments, we place the mannequin at position 10, which is on the border of the LOS and NLOS regions. We then rotate the mannequin orientation in 45 degree increments, run the same motion sequence, and examine the collected signal using 300 masks. The results of this study are shown in Fig. 7. In this figure, *0 degrees* is defined as the orientation in which the mannequin's side faces the DMA, whereas *90 degrees* is defined as the mannequin's chest facing the DMA (the orientation used in prior measurements as well). Since the results for orientations 180 degrees separation are almost identical—the linear motion does not change significantly, and our system does not differentiate front or back— we only report results for 0, 45, 90, and 135 degrees.

As seen in Fig. 7, it becomes easier to detect motion as we turn the mannequin to face the DMA. This is due to the fact that when the mannequin's side is facing the DMA, its profile is much smaller from the transmitter's perspective. This impact is much less pronounced when we use diverse patterns of the DMA, which underlines the utility of the DMA in establishing a high-fidelity sensing scheme. In fact, when using the DMA's diverse patterns, we not only detect motion, but can also correctly characterize the motion periodicity (i.e 0.4 Hz) for all orientations. To confirm the increased fidelity is due to the spatially diverse patterns, we also conducted the same tests with rotated mannequin, but used the same mask 300 times. The comparison between 300 unique masks and 300 identical masks is shown in Fig. 7 Column B, which clearly shows the susceptibility of a non-reconfigurable sensor to orientation of the movement.

F. FURNISHED ROOM

In the studies above, we conducted the test with the room empty. To better emulate actual living conditions, we place

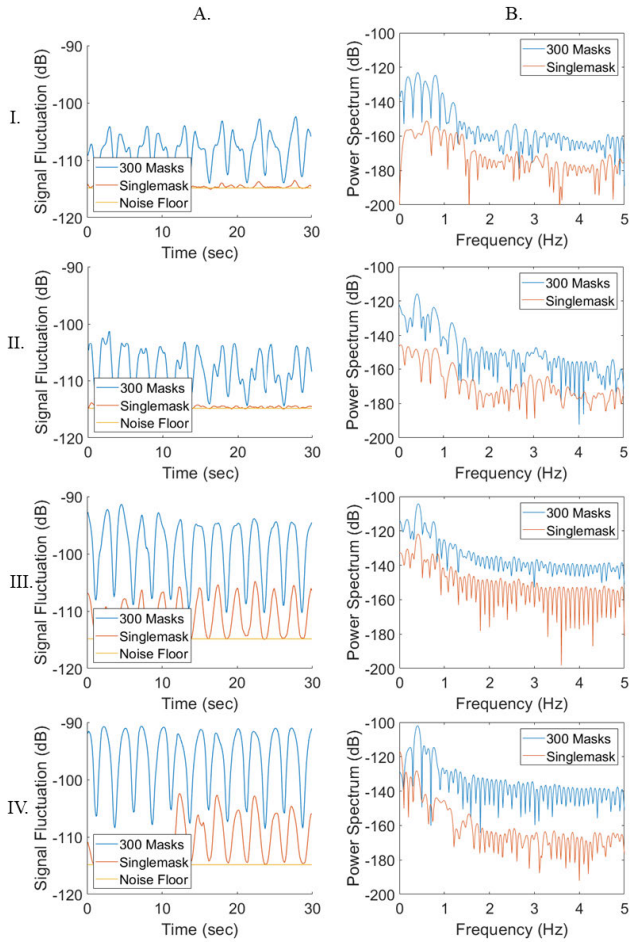

FIGURE 7. Detection fidelity with changing orientation. *Rows: I.* 0 degrees *II.* 45 degrees *III.* 90 degrees *IV.* 135 degrees. *Columns: A.* Smoothed signal fluctuation, 300 masks, singlemask, and still case *B.* Power spectrum, 300 masks and singlemask.

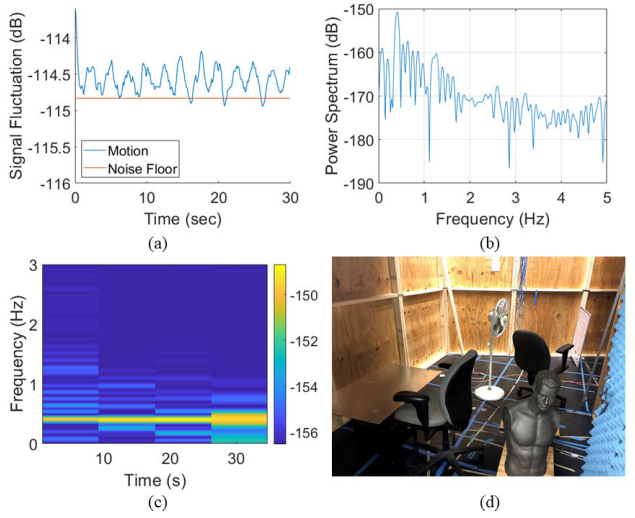

FIGURE 8. Detection fidelity in a cluttered room. (a): Smoothed fluctuation signal. (b): STFT of fluctuation signal. (c): Spectrogram of fluctuation signal. (d): Image of room populated with clutter.

various objects inside the room similar to a furnished residence as seen in (Fig 8d). We then take the same set of measurements at 800 masks with the moving mannequin in location 14, the same location as our NLOS measurements reported in Fig. 4. As illustrated in Figs 8 (a), (b), and (c), the DMA functions equally as well in a ''cluttered'' room. It is important to note that we do not ''recalibrate'' the DMA by taking a new measurement of the cluttered room without motion to compute a new noise floor. This is because the noise floor is inherent to the receiver and does not change as the room changes. Therefore, a commercial sensing scheme based on our DMA setup would only require a single initial measurement at installation to measure the noise floor and, from then on, would be able to adapt to typical changes to the room's variations. There is also a possibility that adding objects actually improves the DMA's detection capabilities as it facilitates its patterns reverberation around the corners to the NLOS locations.

V. SUMMARY AND DISCUSSION

The experimental results presented in this paper demonstrate a DMA's unique application to sensing small movements. We show that by using the DMA's reconfigurable patterns, we can detect motion in both LOS and NLOS locations with high fidelity even at a single frequency. The impact of movement directions, and robustness of the DMA in detecting motion despite such changes, were also investigated. The data further reveal that a DMA sensing scheme can operate even when room configuration changes. Since DMAs have the potential to be tuned rapidly (up to several KHz), they also can capture temporal signatures of the motion. These signatures will be used in future work to distinguish human presence from other sources of motion. With the unique advantages of the DMA-sensing scheme demonstrated in this paper, we believe it can find applications in sensing human presence for intelligently controlling home appliances for saving power. Furthermore, the diverse set of information gathered by the DMA can also be used to classify human activity, which can find applications in smart context-aware homes, such as in monitoring the health of occupants or intruder detection.

In future work, we will explore replacing the printed dipole receiver with another DMA. We have seen the use of a DMA as both transmitter and receiver provides significant improvement in imaging [27], and there is also a possibility that it could improve sensing capabilities. Another interesting study is to examine the locations of the transmitter and receiver, and their impact on the sensing performance. Another option is to conduct measurements in real time on human subjects. While the controlled environment used in this paper provided us with the opportunity to conduct a fair comparison between different scenarios, examining real-time sensing will be an important future direction. Finally, we could also further develop our method of analysis. This paper has primarily focused on demonstrating the utility of using DMAs for sensing and their associated advantages, with rudimentary processing. Applying advanced signal processing techniques or machine learning algorithms could

further improve detection fidelity or yield more information about the source of motion such as its activity, location, and gesture, among other features of interest.

ACKNOWLEDGEMENT

The views and opinions of authors expressed herein do not necessarily state or reflect those of the United States Government or any agency thereof.

REFERENCES

[1] S. Palipana, B. Pietropaoli, and D. Pesch, "Recent advances in RF-based passive device-free localisation for indoor applications," *Ad Hoc Netw.*, vol. 64, pp. 80–98, Sep. 2017.

[2] F. Adib, H. Mao, Z. Kabelac, D. Katabi, and R. C. Miller, "Smart homes that monitor breathing and heart rate," in *Proc. 33rd Annu. ACM Conf. Hum. Factors Comput. Syst. (CHI)*, 2015, pp. 837–846.

[3] J. Lu, T. Sookoor, V. Srinivasan, G. Gao, B. Holben, J. Stankovic, E. Field, and K. Whitehouse, "The smart thermostat: Using occupancy sensors to save energy in homes," in *Proc. 8th ACM Conf. Embedded Netw. Sensor Syst.*, 2010, pp. 211–224.

[4] L. Atzori, A. Iera, and G. Morabito, "The Internet of Things: A survey," *Comput. Netw.*, vol. 54, no. 15, pp. 2787–2805, Oct. 2010.

[5] "2015 residential energy consumption survey (RECS)," U. E. I. Administration, New Delhi, India, Tech. Rep., 2015. [Online]. Available: https://www.eia.gov/consumption/residential/data/2015/c&e/pdf/ce1.1.pdf

[6] L. Z. Rubenstein, "Falls in older people: Epidemiology, risk factors and strategies for prevention," *Age Ageing*, vol. 35, no. 2, pp. ii37–ii41, Sep. 2006.

[7] C.-W. Wang, A. Hunter, N. Gravill, and S. Matusiewicz, "Unconstrained video monitoring of breathing behavior and application to diagnosis of sleep apnea," *IEEE Trans. Biomed. Eng.*, vol. 61, no. 2, pp. 396–404, Feb. 2014.

[8] J. Xiong, F. Li, and J. Liu, "Fusion of different height pyroelectric infrared sensors for person identification," *IEEE Sensors J.*, vol. 16, no. 2, pp. 436–446, Jan. 2016.

[9] H. Liu, Y. Wang, K. Wang, and H. Lin, "Turning a pyroelectric infrared motion sensor into a high-accuracy presence detector by using a narrow semi-transparent chopper," *Appl. Phys. Lett.*, vol. 111, no. 24, Dec. 2017, Art. no. 243901.

[10] I. J. Amin, A. J. Taylor, F. Junejo, A. Al-Habaibeh, and R. M. Parkin, "Automated people-counting by using low-resolution infrared and visual cameras," *Measurement*, vol. 41, no. 6, pp. 589–599, Jul. 2008.

[11] F. Adib, C.-Y. Hsu, H. Mao, D. Katabi, and F. Durand, "Capturing the human figure through a wall," *ACM Trans. Graph.*, vol. 34, no. 6, p. 219, 2015.

[12] M. Zhao, T. Li, M. A. Alsheikh, Y. Tian, H. Zhao, A. Torralba, and D. Katabi, "Through-wall human pose estimation using radio signals," in *Proc. IEEE/CVF Conf. Comput. Vis. Pattern Recognit.*, Jun. 2018, pp. 7356–7365.

[13] E. Yavari, C. Song, V. Lubecke, and O. Boric-Lubecke, "Is there anybody in there?: intelligent radar occupancy sensors," *IEEE Microw. Mag.*, vol. 15, no. 2, pp. 57–64, Mar. 2014.

[14] M. Amin, *Radar for Indoor Monitoring: Detection, Classification, Assessment*. Boca Raton, FL, USA: CRC Press, 2017.

[15] Q. Xu, Y. Chen, B. Wang, and K. J. R. Liu, "Radio biometrics: Human recognition through a wall," *IEEE Trans. Inf. Forensics Security*, vol. 12, no. 5, pp. 1141–1155, May 2017.

[16] B. Wang, Q. Xu, C. Chen, F. Zhang, and K. J. R. Liu, "The promise of radio analytics: A future paradigm of wireless positioning, tracking, and sensing," *IEEE Signal Process. Mag.*, vol. 35, no. 3, pp. 59–80, May 2018.

[17] S. Z. Gurbuz and M. G. Amin, "Radar-based human-motion recognition with deep learning: Promising applications for indoor monitoring," *IEEE Signal Process. Mag.*, vol. 36, no. 4, pp. 16–28, Jul. 2019.

[18] J. A. Nanzer, "A review of microwave wireless techniques for human presence detection and classification," *IEEE Trans. Microw. Theory Techn.*, vol. 65, no. 5, pp. 1780–1794, May 2017.

[19] Y. Li, K. C. Ho, and M. Popescu, "A microphone array system for automatic fall detection," *IEEE Trans. Biomed. Eng.*, vol. 59, no. 5, pp. 1291–1301, May 2012.

[20] P. del Hougne, M. F. Imani, T. Sleasman, J. N. Gollub, M. Fink, G. Lerosey, and D. R. Smith, "Dynamic metasurface aperture as smart Around-the-Corner motion detector," *Sci. Rep.*, vol. 8, no. 1, p. 6536, Dec. 2018.

[21] J. de Rosny, P. Roux, M. Fink, and J. H. Page, "Field fluctuation spectroscopy in a reverberant cavity with moving scatterers," *Phys. Rev. Lett.*, vol. 90, no. 9, Mar. 2003, Art. no. 094302.

[22] S. G. Conti, J. de Rosny, P. Roux, and D. A. Demer, "Characterization of scatterer motion in a reverberant medium," *J. Acoust. Soc. Amer.*, vol. 119, no. 2, pp. 769–776, 2006.

[23] T. Sleasman, M. F. Imani, J. N. Gollub, and D. R. Smith, "Dynamic metamaterial aperture for microwave imaging," *Appl. Phys. Lett.*, vol. 107, no. 20, Nov. 2015, Art. no. 204104.

[24] T. Sleasman, M. F. Imani, W. Xu, J. Hunt, T. Driscoll, M. S. Reynolds, and D. R. Smith, "Waveguide-fed tunable metamaterial element for dynamic apertures," *IEEE Antennas Wireless Propag. Lett.*, vol. 15, pp. 606–609, 2016.

[25] M. F. Imani, J. N. Gollub, O. Yurduseven, A. V. Diebold, M. Boyarsky, T. Fromenteze, L. Pulido-Mancera, T. Sleasman, and D. R. Smith, "Review of metasurface antennas for computational microwave imaging," *IEEE Trans. Antennas Propag.*, vol. 68, no. 3, pp. 1860–1875, Mar. 2020.

[26] M. F. Imani, T. Sleasman, and D. R. Smith, "Two-dimensional dynamic metasurface apertures for computational microwave imaging," *IEEE Antennas Wireless Propag. Lett.*, vol. 17, no. 12, pp. 2299–2303, Dec. 2018.

[27] T. Sleasman, M. Boyarsky, M. F. Imani, T. Fromenteze, J. N. Gollub, and D. R. Smith, "Single-frequency microwave imaging with dynamic metasurface apertures," *J. Opt. Soc. Amer. B, Opt. Phys.*, vol. 34, no. 8, pp. 1713–1726, 2017.

[28] O. S. Mizrahi, M. F. Imani, K. P. Trofatter, J. N. Gollub, and D. R. Smith, "2D ray tracing analysis of a dynamic metasurface antenna as a smart motion detector," *IEEE Access*, vol. 7, pp. 159674–159687, 2019.

[29] O. S. Mizrahi, M. F. Imani, J. N. Gollub, and D. R. Smith, "Generating information-diverse microwave speckle patterns inside a room at a single frequency with a dynamic metasurface aperture," *IEEE Access*, vol. 8, pp. 36829–36835, 2020.

[30] T. Sleasman, M. F. Imani, A. V. Diebold, M. Boyarsky, K. P. Trofatter, and D. R. Smith, "Implementation and characterization of a two-dimensional printed circuit dynamic metasurface aperture for computational microwave imaging," *IEEE Trans. Antennas Propag.*, early access, Oct. 2, 2020, doi: 10.1109/TAP.2020.3027188.

[31] J. N. Gollub, O. Yurduseven, K. P. Trofatter, D. Arnitz, M. F. Imani, T. Sleasman, M. Boyarsky, A. Rose, A. Pedross-Engel, H. Odabasi, T. Zvolensky, G. Lipworth, D. Brady, D. L. Marks, M. S. Reynolds, and D. R. Smith, "Large metasurface aperture for millimeter wave computational imaging at the human-scale," *Sci. Rep.*, vol. 7, no. 1, p. 42650, May 2017.

[32] I. Yoo, M. F. Imani, T. Sleasman, and D. R. Smith, "Efficient complementary metamaterial element for waveguide-fed metasurface antennas," *Opt. Exp.*, vol. 24, no. 25, pp. 28686–28692, 2016.

[33] G. Maret, "Diffusing-wave spectroscopy," *Current Opinion Colloid Interface Sci.*, vol. 2, no. 3, pp. 251–257, 1997.

[34] G. Lerosey and J. de Rosny, "Scattering cross section measurement in reverberation chamber," *IEEE Trans. Electromagn. Compat.*, vol. 49, no. 2, pp. 280–284, May 2007.